# THE KNOTTY QUESTION OF THE JET OF PKS B1421-490

 $J.\ M.\ Gelbord^1,\ H.\ L.\ Marshall^1,\ D.\ M.\ Worrall^{2,3},\ M.\ Birkinshaw^{2,3},\ J.\ E.\ J.\ Lovell^4,\ R.\ Ojha^4,\ L.\ Godfrey^{4,5},\ D.\ A.\ Schwartz^2,\ E.\ S.\ Perlman^6,\ M.\ Georganopoulos^{6,7},\ D.\ W.\ Murphy^8,\ D.\ L.\ Jauncey^4$ 

Accepted to Ap. J. Letters 7 September 2005.

## **ABSTRACT**

We report the discovery of unusually strong optical and X-ray emission associated with a knot in the radio jet of PKS B1421-490. The knot is the brightest feature observed beyond the radio band, with knot/core flux ratios  $\sim \! \! 300$  and 3.7 at optical and X-ray frequencies. We interpret the extreme optical output of the knot as synchrotron emission. The nature of the X-ray emission is unclear. We consider a second synchrotron component, inverse Compton emission from a relativistic, decelerating jet, and the possibility that this feature is a chance superposition of an unusual BL Lac object.

Subject headings: galaxies: jets — quasars: individual (PKS B1421-490)

## 1. INTRODUCTION

We have observed PKS B1421-490 (Ekers 1969) as part of our *Chandra* survey of flat-spectrum radio sources with extended structure (Marshall et al. 2005). A component at  $14^{\rm h}24^{\rm m}32^{\rm s}23$ ,  $-49^{\circ}13'50''0$  (J2000.0) accounts for 93% of the 8.6 GHz flux density; the remaining emission extends  $\sim 12''$  to the south west (Lovell 1997). Gelbord & Marshall (2005) discovered an optical counterpart with  $g'=24.2\pm0.2$  at the position of the radio peak. We estimate the redshift to be  $1 \lesssim z \lesssim 2$  by comparing the g'-r' and r'-i' colors (0.46 and 0.30, respectively, after dereddening) with a sample of SDSS quasars (Richards et al. 2002). An exceptionally bright optical feature (g'=17.8) is coincident with a weak component in the extended radio structure 5."9 from the radio peak. Here we discuss this enigmatic feature in detail.

We adopt z=1,  $H_0=70~{\rm km\,s^{-1}\,Mpc^{-1}}$ ,  $\Omega_{\rm m}=0.3$ , and  $\Omega_{\Lambda}=0.7$ , such that 1" corresponds to 8.0 kpc at the source. We define the power law spectral index  $\alpha$  by  $S_{\nu} \propto \nu^{-\alpha}$ . All uncertainties are 1- $\sigma$  and limits are 2- $\sigma$ .

## 2. OBSERVATIONS

We observed PKS B1421-490 with the Australia Telescope Compact Array (*ATCA*) at 4.86 and 8.64 GHz on 2002 February 4 and at 17.73 and 20.16 GHz on 2004 May 9. The Magellan Instant Camera (MagIC) was used for imaging in the SDSS i', r', and g' filters on 2003 April 26–27, and the Inamori Magellan Areal Camera and Spectrograph (IMACS) was used to obtain a spectrum spanning 4100–7250 Å during twilight on 2004 February 27. X-ray data were obtained on 2004 January 16 using the *Chandra* ACIS-S CCD. Imaging

dwm@sgra.jpl.nasa.gov, David.Jauncey@csiro.au

TABLE 1
PKS B1421-490 FLUX DENSITY MEASUREMENTS

Frequency (Hz)	$S_{ u,\mathrm{A}}^{\mathrm{a}}$ (mJy)	$S_{ u,\mathrm{B}} \ (\mathrm{mJy})$	$S_{ u,C}$ (mJy)
$4.86 \times 10^{9}$	$4980 \pm 10$	< 7	$80 \pm 5$
$8.64 \times 10^{9}$	$3679 \pm 7$	$9.6 \pm 0.6$	$46.1 \pm 0.6$
$1.77 \times 10^{10}$	$2100 \pm 4$	$9.8 \pm 0.3$	$20.6 \pm 0.3$
$2.02 \times 10^{10}$	$1960 \pm 4$	$9.2 \pm 0.2$	$17.5 \pm 0.3$
$1.38 \times 10^{14}$	< 0.37	$1.00 \pm 0.07$	< 0.37
$1.82 \times 10^{14}$	< 0.27	$0.88 \pm 0.06$	< 0.31
$2.40 \times 10^{14}$	< 0.21	$0.91 \pm 0.07$	< 0.36
$3.93 \times 10^{14}$	$(3.9 \pm 0.8) \times 10^{-3}$	$0.81 \pm 0.12$	$< 1.4 \times 10^{-3}$
$4.82 \times 10^{14}$	$(3.0 \pm 0.9) \times 10^{-3}$	$0.78 \pm 0.15$	$< 0.7 \times 10^{-3}$
$6.29 \times 10^{14}$	$(1.9 \pm 0.8) \times 10^{-3}$	$0.73 \pm 0.20$	$< 1.2 \times 10^{-3}$
$2.41 \times 10^{17}$	$(13.3 \pm 1.6) \times 10^{-6}$	$(49 \pm 3) \times 10^{-6}$	$< 1.0 \times 10^{-6}$

NOTE. — Near-IR (from 2MASS; Cutri et al. 2003) and optical flux densities are corrected for Galactic extinction using  $A_K = 0.10$ ,  $A_H = 0.15$ ,  $A_J = 0.24$ ,  $A_{i'} = 0.56$ ,  $A_{r'} = 0.73$ , and  $A_{g'} = 1.01$  (Schlegel, Finkbeiner, & Davis 1998). The optical flux uncertainties are dominated by this correction.

data are presented in Fig. 1 and flux density  $(S_{\nu})$  measurements in Tab. 1.

The radio structure exhibits three main emitting regions (A, B, C on Fig. 1a) spanning 12'' along position angle PA  $\sim 209^{\circ}$ east of north. The 18 and 20 GHz maps resolve region A into a point source and a jet-like extension (A1 and A2, respectively). A2 has FWHM of  $\sim 0.00000$  by 0.00000 extending westward from A1 (PA = 259°) before bending toward regions B and C. (Hereafter, unless A1 or A2 are specified, "region A" will refer to blends or the explicit sum of these two subregions.) At 2.3 GHz Preston et al. (1989) report that A1 contains two VLBI components with ~30 mas diameters separated by 55 mas roughly along the direction to A2. An 8.425 GHz VLBI snapshot taken with the Long Baseline Array (LBA) on 2004 April 16 shows a ~20 mas jet with  $PA \sim 250^{\circ}$ , but formally sets an upper limit of 24 mas on the size of this feature within A1, with  $S_{8.4\,\mathrm{GHz}} = 1.3 \pm 0.3\,\mathrm{Jy}$ . A1 has a flatter radio spectrum than A2. Since it includes some extended flux from the base of A2 and certainly blends the VLBI structures, there is likely to be a component within A1 with a flat or inverted radio spectrum.

<sup>&</sup>lt;sup>1</sup> MIT Kavli Inst. for Astrophysics and Space Research, Massachusetts Inst. of Technology, 77 Massachusetts Ave., Cambridge, MA 02139, USA

<sup>&</sup>lt;sup>2</sup> Harvard-Smithsonian Center for Astrophysics, 60 Garden St., Cambridge, MA 02138, USA

<sup>&</sup>lt;sup>3</sup> Dept. of Physics, U. of Bristol, Tyndall Ave., Bristol BS8 1TL, UK

<sup>&</sup>lt;sup>4</sup> CSIRO ATNF, PO Box 76, Epping, NSW 2121, Australia

<sup>&</sup>lt;sup>5</sup> Research School of Astronomy & Astrophysics, Australian National U.

<sup>&</sup>lt;sup>6</sup> Joint Center for Astrophysics and Physics Dept., U. of Maryland, Baltimore County, 1000 Hilltop Circle, Baltimore, MD 21250, USA
<sup>7</sup> Goddard Space Flight Center, Code 661, Greenbelt, MD 20771, USA

<sup>&</sup>lt;sup>8</sup> Jet Propulsion Lab., 4800 Oak Grove Dr., Pasadena, CA 91109, USA Electronic address: jonathan@space.mit.edu, hermanm@space.mit.edu, D.Worrall@bristol.ac.uk, Mark.Birkinshaw@bristol.ac.uk, Jim.Lovell@csiro.au, Roopesh.Ojha@csiro.au, lgodfrey@mso.anu.edu.au, das@head-cfa.harvard.edu, perlman@jca.umbc.edu, markos@milkyway.gsfc.nasa.gov,

<sup>&</sup>lt;sup>a</sup>At 18 and 20 GHz, region A is resolved into A1 and A2. The tabulated flux densities refer to A1;  $S_{\nu,A2}=600$  and 550 mJy at 18 and 20 GHz, respectively. At other frequencies the  $S_{\nu,A}$  values blend regions A1 and A2.

2 Gelbord et al.

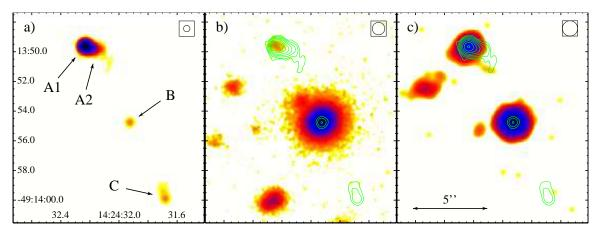


FIG. 1.— PKS B1421-490 imaged in radio, optical, and X-ray bands. a) ATCA radio map at 20.16 GHz, convolved to a circular beam with 0."44 FWHM. The map peaks at 2.14 Jy/beam and has a background RMS level of 0.129 mJy/beam. b) Magellan i' image (smoothed to 0."86 FWHM) with radio contours corresponding to panel (a). The contour levels are separated by factors of three starting from 7× the background RMS. The astrometric solution, based upon 29 field stars listed in the GSC 2.2.01, yields an offset of <0."1 between the radio and optical centroids at A1. c) Chandra 0.5-7.0 keV image (convolved to 1."03 FWHM) with overlaid radio contours. The logarithmic stretch spans 0.75-266 counts/beam. A shift by ~0."3 has been applied to register the northern peak with A1. All images are shown at the same angular scale, with the beam FWHM sizes indicated. Region B is slightly resolved in the radio map but not in the optical or X-ray images, where it becomes the dominant component. The offsets between the radio, optical, and X-ray peaks at B are negligible (<0."1).

Region B lies 5."9 from A1 in PA = 211°. It is the weakest of the labeled radio features, with only 0.4% of the overall flux density of region A at 20 GHz. The 18 and 20 GHz data show it to be resolved (the deconvolved FWHM is  $0.12\pm.03$  by  $0.09^{+.03}_{-.05}$  with the major axis in PA =  $21^{+21}_{-12}$  deg.). At 4.8 GHz C is sufficiently extended to contaminate region B.

Region C is well resolved, reaching its peak brightness at its southernmost end, 11."5 from A1 at PA = 208°. It has a steep spectrum ( $\alpha_{\rm r,C}$  = 1.15  $\pm$  0.03 between 8.6 and 20 GHz), in contrast to the flat spectra of A and B ( $\alpha_{\rm r,A}$  = 0.448  $\pm$  0.005 and  $\alpha_{\rm r,B}$  = 0.05  $\pm$  0.10).

Above  $10^{14}$  Hz (Fig. 1b & c), B is the brightest component and C is undetected. The  $S_B/S_A$  flux ratios are 3.7 in the X-ray band and  $\sim 300$  in the optical, contrasting with  $3\times 10^{-3}$  at 8.6 GHz. Both A and B are unresolved, with FWHM upper limits of 0."24 at  $10^{14}$  Hz, and 0."61 and 0."39 (respectively) at  $10^{17}$  Hz. The spectral energy distribution (SED) of A appears to steepen in the optical band ( $\alpha_o = 1.49^{+0.70}_{-0.67}$ ), while that of B remains flat ( $\alpha_o = 0.22 \pm 0.23$ ). Details of the optical data are given by Gelbord & Marshall (2005).

The  $\dot{X}$ -ray spectra of components A and B are both well described by absorbed power laws. We use the maximum likelihood method to fit models to the 0.5–7.0 keV spectra. For component B we find  $\alpha_x=0.42^{+0.24}_{-0.22}$  and a neutral gas column of  $N_H=1.0^{+0.7}_{-0.5}\times 10^{21}$  cm $^{-2}$ , consistent with the  $N_H$  predicted from Galactic H I measurements (1.62 × 10<sup>21</sup> cm $^{-2}$ ; Dickey & Lockman 1990). For region A we obtain  $\alpha_x=0.31^{+0.32}_{-0.31}$  after fixing  $N_H=1.62\times 10^{21}$  cm $^{-2}$ .

An unidentified optical and X-ray source (CXOU J142432.5-491352) lies 4."1 SE of A1. It has flux densities of  $9.2\pm1.5$ ,  $7.5\pm1.7$ , and  $6.5\pm2.1~\mu\mathrm{Jy}$  in the i', r', and g' bands, respectively, and  $3.1\pm0.8~\mathrm{nJy}$  at 1 keV. The density of background X-ray sources at least this bright ( $\mathrm{F}_{2-10\,\mathrm{keV}}=3\times10^{-14}~\mathrm{erg\,cm^{-2}\,s^{-1}}$ , assuming  $\alpha_{\mathrm{x}}=0.6$  and Galactic N<sub>H</sub>) is about 100 per square degree (Rosati et al. 2002; Moretti et al. 2003), so the likelihood of finding one within 10" of at least one of our 30 survey targets observed to date is >7%. The low Galactic latitude of 1421-490 ( $b=10.9^{\circ}$ ) increases the likelihood that this is an unrelated source. A weak optical source lies 1."8 NE of B ( $g'=23.1\pm0.3$ ,  $r'=22.5\pm0.2$ , and

 $i' = 22.0 \pm 0.2$  with no extinction correction). It lacks any radio or X-ray counterpart and is consistent with a point source, hence is likely to be a foreground star in this crowded field. We do not discuss either object further.

## 3. DECIPHERING THE MORPHOLOGY

We suggest that region C is a terminal hot spot due to its extended radio structure and steep spectrum. The knotty question is whether we have a core at A with a one-sided jet extending through B to C or a symmetric system with a core at B between hot spots at A and C. The radio spectral indices do not provide guidance because both A and B have flat spectra typical of self-absorbed quasar cores. The detection of a compact, high brightness temperature VLBI source with apparent core-jet morphology coincident with A1 is suggestive but not conclusive: a hot spot could contain a compact component, although it would be exceptional for it to have core-jet structure and to provide so much (35%) of the  $\sim$ 8.5 GHz flux density. The lack of a VLBI source at B is likewise not significant because B would not have been detected by extant observations. For now we adopt the one-sided jet scenario, guided by the VLBI source at A1. This choice may need to be reconsidered as new data become available. However, we note that  $\alpha_{r,A1} < \alpha_{r,A2}$ , consistent with a core/inner jet interpretation.

One other possibility warrants consideration: that A and B are cores in separate systems. In comparison with other jet knot-core pairs, the B/A X-ray flux ratio is atypical and the optical ratio unprecedented. Given that X-ray sources with  $F_{2-10\,\mathrm{keV}} \geq 4.3 \times 10^{-13}\,\mathrm{erg\,cm^{-2}\,s^{-1}}$  have a density of  $\sim\!1.0$  per square degree (Moretti et al. 2003), the chance of finding such a source  $<\!10''$  from any of the systems so far observed in our jet survey is  $\sim\!7.3 \times 10^{-4}$  if we neglect the possibility of clustering. Thus it is unlikely that A and B are unrelated.

We obtained an optical spectrum (Fig. 2) to test whether B is an interloper. Only one tentative feature, an absorption line at 5825Å, exceeds  $4\times$  the local RMS. A redshift limit of z < 2.6 is required by the absence of a Lyman forest at  $\lambda > 4370$ Å. The lack of strong spectral features rules out identification with common objects such as normal stars, galaxies and most types of AGN, and is consistent with non-thermal

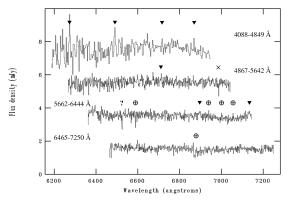


FIG. 2.— IMACS spectrum of region B. From the top down the spectral segments have been shifted by 2100, 1400, 700 & 0 Å and by 6, 4, 2 & 0 mJy. Residual telluric features ( $\oplus$ ), cosmic rays ( $\blacktriangledown$ ), and a bad column at 5587 Å ( $\times$ ) are marked. The spectral resolution is  $\Delta\lambda=3.5$  Å except for the bluest segment which is rebinned to  $\Delta\lambda=7.0$  Å. The spectrum has been dereddened assuming A<sub>V</sub> = 0.884 (Schlegel et al. 1998). The most significant feature is a tentative absorption line at 5825 Å (marked with "?"), which represents a dip from the continuum by 4.3 $\times$  the local RMS. A Lyman forest can be ruled out for  $\lambda>4370$  Å, confirming that z<2.6.

emission from a jet knot. The only remaining candidates are DC white dwarfs (WDs) and BL Lac objects. The former can be dismissed immediately as these cool WDs are neither radio nor X-ray sources and are generally bluer (r'-i' < 0.00, e.g., Kleinman et al. 2004, whereas B has r'-i' = 0.21). Moreover, photographic plates from the Yale/San Juan Southern Proper Motion survey (SPM; Girard et al. 2004) limit the proper motion of B to <8 mas yr $^{-1}$  (D. I. Dinescu 2004, private communication); with a distance <150 pc (based upon the brightest known DC WDs; McCook & Sion 1999) the tangential motion is limited to T < 6 km s $^{-1}$  whereas WDs typically have  $T = 55 \pm 45$  km s $^{-1}$  (Sion et al. 1988).

If B is a BL Lac, then it is highly unusual. Its  $\alpha_{rx}$  index is typical of X-ray-selected BL Lacs, but  $\alpha_{ro}$  and  $\alpha_{ox}$  (< 0.20 and 1.62, respectively<sup>9</sup>) are exceptional, making B an outlier when compared to published samples (Worrall et al. 1999; Rector et al. 2000; Landt et al. 2001). However, other methods of selection may broaden the distribution of indices—e.g., the optically-selected, radio-quiet BL Lac candidate discovered by Londish et al. (2004). BL Lac objects typically vary in the optical by a magnitude or more on time scales of years, but catalogs and archival data<sup>10</sup> show  $\Delta B_i < 0.6$  over 35 yr and < 0.3 on time scales up to 27 yr. Finally, BL Lacs with comparable X-ray fluxes are rare: the chance of having one within 10" of any of our 30 Chandra targets is  $< 1.5 \times 10^{-4}$ (Wolter et al. 1991; Krautter et al. 1999; Henry et al. 2001); finding one aligned with a radio jet is even less likely. Thus, while we cannot completely rule out a BL Lac interloper, we favor an association of B with PKS B1421-490.

The multiwavelength properties of feature B are unlike those of any other known jet knot. Its optical apparent magnitude is second only to knot HST-1 of M87 despite lying at a much greater distance. HST-1 has a comparable X-ray  $S_{knot}/S_{core}$  ratio, but its optical ratio is 3, compared to  $\sim\!300$  for knot B (Marshall et al. 2002; Harris et al. 2003).

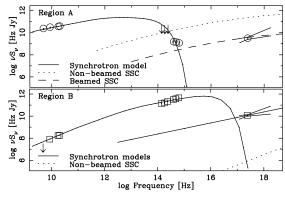


FIG. 3.— Spectral energy distributions (SED) and models of the core (region A; top) and knot B (bottom). Synchrotron models (solid curves) are drawn through the radio and optical fluxes of both sources. For the core, a synchrotron self-Compton (SSC) model with significant bulk relativistic motion (dashed line) gives a good fit to the X-ray flux, whereas a non-relativistic SSC model (dotted line) is too high. For the knot, the predicted SSC contribution is far too low; it would be suppressed further if a high  $\gamma_{min}$  or a hardened electron distribution is invoked to accommodate the S<sub>4.8GHz</sub> limit. An ad hoc second synchrotron component with a typical slope ( $\alpha$  = 0.5) could work, matching the X-ray data while contributing negligibly at lower frequencies.

#### 4. INTERPRETING THE SPECTRA

The core SED can be modeled as emission from the parsec-scale base of the jet. The spectral index of A1 between 17.7 and 20.2 GHz is 0.5, roughly consistent with strong-shock acceleration models. A synchrotron self-Compton (SSC) model with an equipartition magnetic field ( $B_{\rm eq}$ ) is plausible for the core as long as there is relativistic boosting towards the observer. For example, Fig. 3 shows a model of a jet with bulk motion of  $\Gamma=20$  at  $2.9^{\circ}$  to the line of sight, radius 0.5 mas (4 pc), electron number spectrum index p=2.0,  $\gamma_{\rm min}=20$ ,  $\gamma_{\rm max}=1.3\times10^4$ , and an energy-loss break by 1.0 at  $\gamma=1.6\times10^3$ . Such a model gives a reasonable description of the SED with  $B_{\rm eq}=13$  mG. Without relativistic beaming SSC models with  $B\approx B_{\rm eq}$  predict an X-ray flux  $\sim 70\times$  higher.

For region B we also use synchrotron emission to model the radio-to-optical flux. The flat spectrum and apparent turnover at low radio frequencies might suggest self-absorption in a series of small-scale components. This is often the case in cores but not large-scale jets. While there could be a selfabsorbed region within the kpc-scale knot if the magnetic field is sufficiently high ( $\sim$ mG), we prefer instead an optically thin model. Without beaming, a model consisting of a sphere of radius 0."05 (0.4 kpc), with  $B_{eq} = 0.86$  mG, p = 1.0,  $\gamma_{min} = 20$ ,  $\gamma_{\text{break}} = 1 \times 10^5$ , and  $\gamma_{\text{max}} = 3 \times 10^6$ , yields a reasonable fit (Fig. 3), although it violates the  $S_{4.8GHz}$  limit and it is difficult to reproduce  $\alpha_{\rm o} < 0.5$  unless p < 2.0 above  $\gamma_{\rm break}$ . An unusually high  $\gamma_{\min}$  ( $\sim 2 \times 10^4$ ) would provide a better compromise between the flat 8.6-20 GHz radio spectrum and the low 4.8 GHz flux density, although the physical mechanism would be uncertain;  $B_{eq}$  would be little changed. The flatness of the optical spectrum suggests that the electron distribution would be better modelled as multiple components with a distribution of  $\gamma_{\rm max}$  values. The radiative lifetime of the optically-emitting electrons is only of order 40 years, implying distributed electron acceleration across the knot. Smaller electron Lorentz factors apply if the source size is reduced.

The greater difficulty is to explain the X-ray emission. Unlike the core, the relatively larger angular size and lower radio luminosity of the knot means that SSC is not effective unless

<sup>&</sup>lt;sup>9</sup> Evaluated with the upper limit at 4.8 GHz and extrapolated  $S_{\nu}$  values at 2500 Å and 2 keV to facilitate comparison with Rector et al. 2000.

<sup>&</sup>lt;sup>10</sup> The USNO-A2.0 (Monet et al. 1998), USNO-B1.0 (Monet et al. 2003) and HST GSC 2.2 (http://www-gsss.stsci.edu/gsc/GSChome.htm) catalogs, and the SPM survey (D. I. Dinescu 2004, private communication).

4 Gelbord et al.

most of the radio emission is from embedded regions smaller than we adopt for the core. The observed flux is too low to be a simple continuation of the optical synchrotron and too flat to be the plunging high-energy tail of this component. Synchrotron X-ray emission requires a second population of electrons extending to  $\gamma \gtrsim 10^7$  with  $1.4 \lesssim p \lesssim 2.3$ . The resulting emission extrapolates well below the fluxes measured at lower frequencies, thus  $\gamma_{\min}$  is unconstrained. *In situ* acceleration is required to sustain this population as the cooling time is much shorter than the light-crossing time of the region.

Inverse Compton (IC) models likewise have problems reproducing the knot X-ray emission. IC scattering of the cosmic microwave background (IC-CMB; Tavecchio et al. 2000; Celotti, Ghisellini, & Chiaberge 2001) for  $B=B_{\rm eq}$  requires a bulk Lorentz factor  $\Gamma>60$  to boost the X-ray output by 8 orders of magnitude. This is inconsistent with our expectation that the knot should be less boosted than the core, especially after a bend in the jet as between A2 and B. A higher assumed redshift would ease this constraint, since  $\Gamma \propto (1+z)^{-(3+\alpha)/(1+\alpha)}$  (Harris & Krawczynski 2002), but even at  $z=z_{\rm max}=2.6$  we require  $\Gamma>24$ . This limit could be reduced to  $\Gamma\lesssim 20$  if magnetic fields significantly below  $B_{\rm eq}$  are considered.

A decelerating jet model (Georganopoulos & Kazanas 2003) with a lower  $\Gamma$  and  $B \approx B_{\rm eq}$  can provide a qualitatively correct SED. A  $\Gamma=20$ , B=0.1 mG flow oriented 2.9° from our line of sight that decelerates to semi-relativistic velocities within the R=0.4 kpc volume of knot B reproduces the optical flux with a strongly Doppler-boosted synchrotron peak and provides X-rays through IC scattering of photons from the slowed, downstream portion of the jet.

Both IC models require abundant  $\gamma \sim 100$  electrons to produce X-rays. These electrons can be in a second population (this time at low energies), or part of the synchrotron-emitting population if  $\gamma_{\rm min}$  is much lower than the assumed value of  $1.6 \times 10^4$ . A low  $\gamma_{\rm min}$  would require the knot to contain unusually compact, self-absorbed sub-regions to avoid producing an order of magnitude more radio flux than observed.

#### 5. CONCLUSIONS

We have chosen to interpret PKS B1421-490 as a flat spectrum radio source with a one-sided jet and a unique knot at B. The optically-dominated spectral energy distribution of feature B can be explained by two models. Both invoke a synchrotron component for the radio-to-optical continuum, but one attributes the X-ray flux to synchrotron emission from a second electron population while the other involves inverse Compton scattering by a relativistic, decelerating jet. Alternative interpretations that currently cannot be ruled out include a symmetric system with a core at B and knots at A and C, and either an interaction, or a chance alignment, of PKS B1421-490 and an unrelated (and unusual) optically-dominated, radio-quiet BL Lac.

Deeper optical spectroscopy is urgently needed to measure the redshift of A and provide a high S/N spectrum to better identify B. Observations in the mm, sub-mm, IR and far-UV bands would fill in the SED, thereby providing strong constraints for models of the emission processes. Feature B is a good target for optical polarimetry, which could help confirm whether it is dominated by synchrotron jet emission. Finally, we look forward to an upcoming long *Chandra* observation that will allow a more detailed X-ray study and a deep VLBI mapping that will test the core-jet structure at A1 and possibly identify compact emission regions within B.

The authors thank Bill van Altena, Dana Dinescu and Terry Girard for their assistance with the SPM archive. This work has been supported in part under SAO contracts GO4-5124, SV1-61010, and NAS8-39073, and NASA LTSA grant NAG5-9997. The ATCA and the LBA are part of the Australia Telescope which is funded by the Commonwealth of Australia for operation as a National Facility managed by CSIRO. This research has made use of the NASA/IPAC Extragalactic Database (NED), NASA's Astrophysics Data System (ADS), and data from the HST Guide Star Catalog (GSC, produced at STScI under U.S. Government grant).

## REFERENCES

Celotti, A., Ghisellini, G., & Chiaberge, M. 2001, MNRAS, 321, L1 Cutri, R. M., et al. 2003, VizieR Online Data Catalog, 2246, 0, (2MASS All-Sky Catalog)

Dickey, J. M., & Lockman, F. J. 1990, ARA&A, 28, 215

Ekers, J. A. 1969, Au. J. of Phys. Astrophys. Supp., 7, 3

Gelbord, J. M., & Marshall, H. L. 2005, in prep.

Georganopoulos, M., & Kazanas, D. 2003, ApJ, 589, L5

Girard, T. M., Dinescu, D. I., van Altena, W. F., Platais, I., Monet, D. G., & López, C. E. 2004, AJ, 127, 3060

Harris, D. E., Biretta, J. A., Junor, W., Perlman, E. S., Sparks, W. B., & Wilson, A. S. 2003, ApJ, 586, L41

Harris, D. E., & Krawczynski, H. 2002, ApJ, 565, 244

Henry, J. P., Gioia, I. M., Mullis, C. R., Voges, W., Briel, U. G., Böhringer, H., & Huchra, J. P. 2001, ApJ, 553, L109

Kleinman, S. J., et al. 2004, ApJ, 607, 426

Krautter, J., et al. 1999, A&A, 350, 743

Landt, H., Padovani, P., Perlman, E. S., Giommi, P., Bignall, H., & Tzioumis, A. 2001, MNRAS, 323, 757

Londish, D., Heidt, J., Boyle, B. J., Croom, S. M., & Kedziora-Chudczer, L. 2004, MNRAS, 352, 903

Lovell, J. E. J. 1997, PhD thesis, University of Tasmania

Marshall, H. L., Miller, B. P., Davis, D. S., Perlman, E. S., Wise, M., Canizares, C. R., & Harris, D. E. 2002, ApJ, 564, 683

Marshall, H. L., et al. 2005, ApJS, 156, 13

McCook, G. P., & Sion, E. M. 1999, ApJS, 121, 1

Monet, D. B. A., et al. 1998, The USNO-A2.0 Catalogue (Washington, DC: U.S. Naval Observatory)

Monet, D. G., et al. 2003, AJ, 125, 984

Moretti, A., Campana, S., Lazzati, D., & Tagliaferri, G. 2003, ApJ, 588, 696 Preston, R. A., et al. 1989, AJ, 98, 1

Rector, T. A., Stocke, J. T., Perlman, E. S., Morris, S. L., & Gioia, I. M. 2000, AJ, 120, 1626

Richards, G. T., et al. 2002, AJ, 123, 2945

Rosati, P., et al. 2002, ApJ, 566, 667

Schlegel, D. J., Finkbeiner, D. P., & Davis, M. 1998, ApJ, 500, 525

 Sion, E. M., Fritz, M. L., McMullin, J. P., & Lallo, M. D. 1988, AJ, 96, 251
 Tavecchio, F., Maraschi, L., Sambruna, R. M., & Urry, C. M. 2000, ApJ, 544, L23

Wolter, A., Gioia, I. M., Maccacaro, T., Morris, S. L., & Stocke, J. T. 1991, ApJ, 369, 314

Worrall, D. M., Birkinshaw, M., Remillard, R. A., Prestwich, A., Tucker, W. H., & Tananbaum, H. 1999, ApJ, 516, 163